Axially twisted chiral nematic structures in cylindrical cavities

M. Ambrožič[1] and S. Žumer[1,2]
[1]*J. Stefan Institute, Jamova 39, SI-1000 Ljubljana, Slovenia*
[2]*Physics Department, University of Ljubljana, Jadranska 19, SI-1000 Ljubljana, Slovenia*
(Received 29 October 1998)

Here we report a theoretical study of chiral nematic liquid crystals, confined to cylindrical cavities with planar anchoring conditions. Three different model structures are considered: radially twisted, eccentric radially twisted, and axially twisted structure. The Frank-Oseen free energy with additional surface energy terms is used to find nematic director fields and free energies of the structures in different ranges of material parameters. We are particularly interested in the influence of chirality, anchoring strength, and the saddle-splay elastic constant on the stability regions of the described structures. For low chiralities the radially twisted structure is stable, while for high chiralities the axially twisted structure is stable. The stability region of the eccentric radially twisted structure is confined to a limited intervals of anchoring strengths and chiralities. Most of our attention is devoted to details of the axially twisted structure. In the high chirality limit the axially twisted structure resembles a simpler model structure which in our previous work we called an asymmetric conical structure. The tilt of the nematic director of the axially twisted structure out of the plane perpendicular to the cylinder axis is small except in the layer at the cylinder boundary. Polarization microscopy simulations of the three structures are also shown. [S1063-651X(99)08504-9]

PACS number(s): 61.30.Cz

I. INTRODUCTION

Chiral nematic liquid crystals in confined geometry have recently attracted a lot of attention. In addition to a large number of studies devoted to electro-optical properties of such systems, several experimental and theoretical investigations have been performed on chiral liquid crystals confined to cylindrical and spherical geometries [1–8]. Membranes (Anopore [9], Nuclepore [10]) with submicrometer cylindrical pores of nearly the same radius are available for detailed studies of highly curved confinement. In cylindrical cavities with planar surface anchoring different model structures have been suggested, among which the double twisted (radially twisted) [11] and helical structures [12], characteristic of unconfined chiral nematics, are the best known. Generally it was believed that, for low chirality (or small cylinder radius), the radially twisted structure was stable while for higher chiralities (or large cylinder radius), the helical structure was stable [1]. In the radially twisted structure (commonly known as the double twisted structure) the nematic director rotates around any axis perpendicular to the cylinder axis [Fig. 1(a)]. In the helical structure the nematic director field is aligned in planes perpendicular to the cylinder axis (helical planes) which are rotated with respect to each other around the cylinder axis. The qualitative features of the structures depend on the ratio of the cylinder radius to the helical pitch, rather than on the radius and the chirality separately [5–8]. A high radius-to-pitch ratio is achieved for chiral nematics in supramicrometer capillary tubes [5,6], while this ratio is lower in cavities of Anopore membranes [7]. According to recent experimental results, different modifications of simple radially twisted and helical structures have been suggested [5–8].

Particularly for higher chiralities, qualitatively different structures were suggested. Ondris-Crawford *et al.* [7] investigated chiral nematics in Anopore membranes. NMR measurements revealed planarlike structures in the high-chirality limit. Therefore, axially twisted planar bipolar (ATPB) structure was suggested. The nematic director field in this structure lies in planes perpendicular to the cylinder axis. Contrary to a simple helical structure, the director field in helical planes is curved. The bipole symmmetry axis in helical planes rotates around the cylinder axis. On the other hand, in submicrometer cylindrical pores Schmiedel *et al.* [5] observed a significant tilt of the nematic director with respect to helical planes, and they suggested a simple model of conical structure where the tilt angle depends only on the distance from cylinder axis. In this structure there is a rotation of the nematic director field around the cylinder axis, as in the case of helical structure.

Stimulated by these experiments, we performed a theoretical analysis of various chiral nematic model structures in submicrometer cylinders with planar anchoring [8]. We showed that the simple conical structure [5] is never stable. Therefore, we suggested an asymetric conical (AC) structure as a generalization of the simple conical (SC) structure. The out-of-plane tilt increases on approaching the surface, but there is no azimuthal (in-plane) bend of nematic director. Contrary to the SC structure, the tilt angle also depends on the azimuthal angle in the helical plane. We found the radially twisted (RT) structure to be stable for low chiralities, while for high chiralities the AC structure is stable. The difference between the AC structure and the simple helical structure was shown to be small.

Here we show how the AC structure in a long cylindrical cavity can be adapted to decrease the free energy further. This more general defectless structure also has an azimuthal component of the nematic director, thus allowing better matching to planar anchoring at the cylinder boundary [Fig. 1(c)]. This structure has features partly of ATPB and partly of AC structures. To avoid further complications with terminology, we decided to simply call this structure an axially

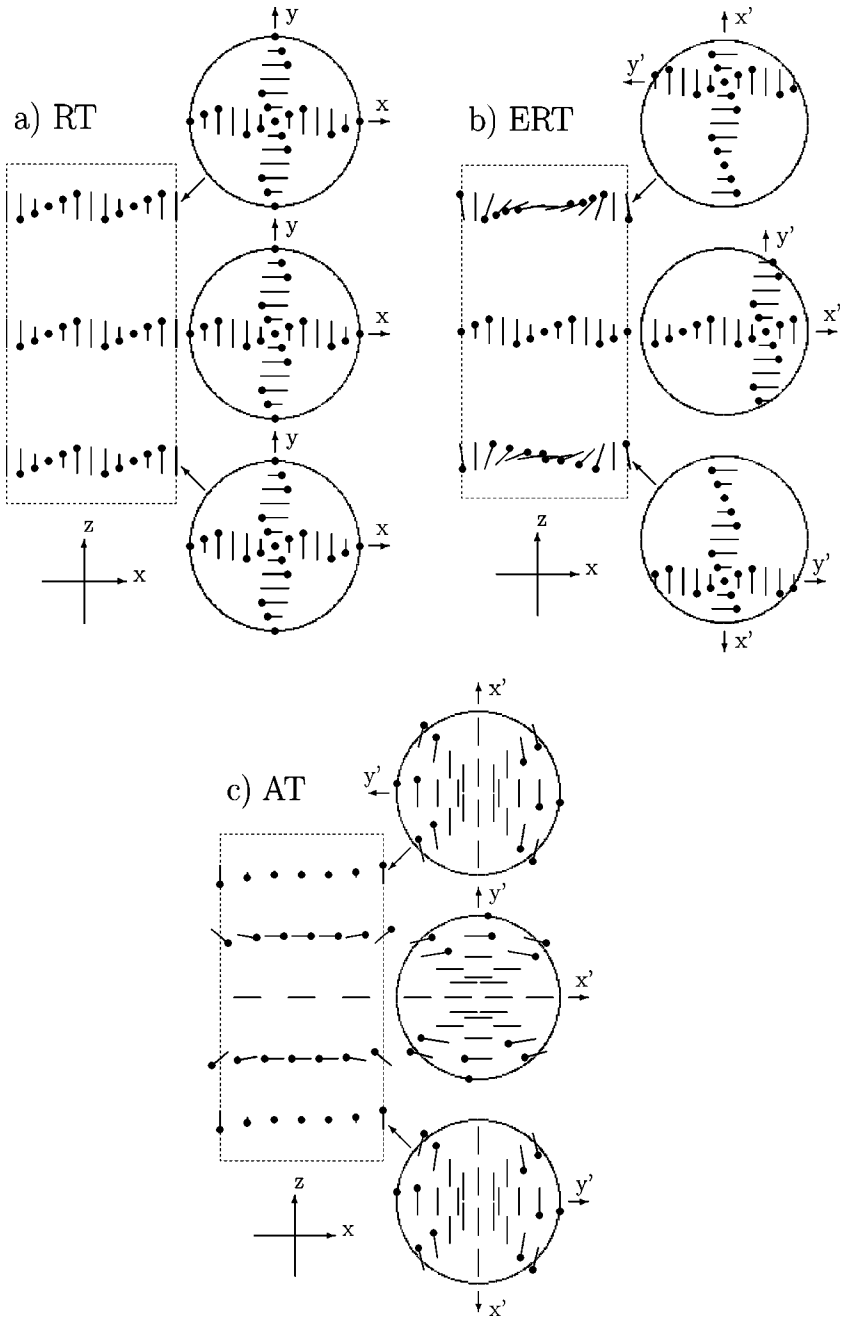

FIG. 1. Schematic representation of three different structures. (a) Radially twisted structure. (b) Eccentric radially twisted structure, with $r_h=0.5R$. (c) Axially twisted structure. The nematic director fields in the cylinder (x,z) plane (left figures) and (x,y) plane [and planes parallel to (x,y) planes; right figures] are shown. The heads of the ''sticks'' indicate the inclination of the nematic director below the plane. The directions of the laboratory coordinate system x, y, and z axes and of the rotating x' and y' axes are indicated.

twisted (AT) structure. Further, we show that our completely optimized AT structure can, in its stability region, be satisfactorily approximated with the simpler AC strucure. This means that the tilt of the nematic director out of the helical planes is much more important than the bend in the planes. Finally we briefly examine changes of the stability limits at low chiralities where the RT structure becomes stable. The importance of the K_{24} free energy term is revealed even for a large cylinder radius (or high chirality limit). In addition, we include a brief description of a so called eccentric radially twisted (ERT) structure [Fig. 1(b)], which at certain range of chiralities is more stable than the simple radially twisted structure [1,6].

One of the most important features of chiral nematic structures is their twist character. RT and ERT structures have essentially a double-twist character, with two local twist axes with equal or comparable chiralities. On the other hand AT and also AC structures are twisted around the cylinder axis, with an additional rather small local twist component about the axis in the plane perpendicular to the cylinder axis.

In Sec. II, theoretical grounds for our phenomenological description of common chiral nematic structures are laid down. In Sec. III, we examine relevant solutions of the

Euler-Lagrange equations for two angles, describing the nematic director fields. In Sec. IV, we discuss results and give a conclusion.

II. FREE ENERGY

Our chiral nematic is described by a nematic director field $\vec{n}(\vec{r})$ with $\vec{n}$ to $-\vec{n}$ equivalence. We neglect the biaxiallity and space variation of the scalar nematic-order parameter, which is a reasonable approximation for defectless structures even in cylinders with submicrometer radia [13].

Cylindrical coordinates r, ϕ, and z are used in our calculations, where the z direction is along the cylinder axis. Unit vectors of the cylindrical coordinate system are denoted by $\vec{e}_r$, $\vec{e}_\phi$, and $\vec{e}_z$. The free energy of a chiral nematic liquid crystal in a cavity is divided into bulk and surface terms:

$$F=\int f_V dV+\int f_S dS. \tag{1}$$

The bulk Frank-Oseen elastic free energy density [14] is written as

$$f_V=\tfrac{1}{2}[K_{11}(\vec{\nabla}\cdot\vec{n})^2+K_{22}(\vec{n}\cdot\vec{\nabla}\times\vec{n}+q)^2+K_{33}(\vec{n}\times\vec{\nabla}\times\vec{n})^2 - K_{24}\vec{\nabla}\cdot(\vec{n}\times\vec{\nabla}\times\vec{n}+\vec{n}\vec{\nabla}\cdot\vec{n})], \tag{2}$$

where K_{11}, K_{22}, and K_{33} are the splay, twist, and bend elastic constants, respectively, and K_{24} is the saddle-splay elastic constant. We use an approximation of equal bulk elastic constants ($K_{11}=K_{22}=K_{33}\equiv K$), while K_{24} is allowed to vary. We omit the K_{13} (splay-bend) energy term. We use the term ''natural chirality'' for the chirality parameter q to stress the difference from the ''actual chirality'' q' in the confined geometry.

In the case of homogeneous planar anchoring with a preferred z direction, the surface free energy density in the Rapini-Papoular approximation [15] is a sum of polar (out-of-plane) and azimuthal (in-plane) surface elastic couplings:

$$f_S=\tfrac{1}{2}(W_\phi\sin^2\psi_S+W_\theta\cos^2\psi_S)\sin^2\theta_S, \tag{3}$$

where W_ϕ and W_θ are the azimuthal and polar anchoring strengths, respectively, θ_S is the angle between the nematic director at the cylinder boundary and the z axis, and ψ_S is the angle between the $(\vec{n},\vec{e}_z)$ and $(\vec{e}_r,\vec{e}_z)$ planes. In the case of degenerate planar anchoring, the strength W_ϕ is zero.

To describe periodic chiral nematic structures (axially twisted structure, etc.), the nematic director field is written as:

$$\vec{n}=\sin\theta(r,\phi')\cos\psi(r,\phi')\vec{e}_r+\sin\theta(r,\phi')\sin\psi(r,\phi')\vec{e}_\phi+\cos\theta(r,\phi')\vec{e}_z, \tag{4}$$

where the helical twist of the nematic director about the cylinder z axis is incorporated in the shifted azimuthal angle $\phi'=\phi-q'z$. This is the most general form of the nematic director field with a uniform twist around the z axis. θ is the angle between the nematic director and the cylinder axis, and ψ is the angle between the projection of nematic director in the (x,y) plane and the unit vector $\vec{e}_r$. At the cylinder boundary the angles θ and ψ agree with the angles θ_S and ψ_S [Eq. (3)], respectively.

We denote by x' and y' the Cartesian coordinates and axes of the coordinate system, which rotates around cylinder axis according to the chirality q'. This is consistent with the helical director field $(\cos q'z,\sin q'z,0)$ in Cartesian coordinates. The actual chirality q' is generally different from the natural chirality q. This is expected since the chirality of the nematic liquid crystal can impose a local twist in another direction, not only around the cylinder axis.

We introduce dimensionless (''reduced'') quantities for the radius vector, chiralities, K_{24} elastic constant, anchoring strengths, and free energy:

$$\rho=\frac{r}{R}, \tag{5}$$

$$\mathcal{Q}=qR, \tag{6}$$

$$\mathcal{Q}'=q'R, \tag{7}$$

$$\mathcal{K}_{24}=K_{24}/K, \tag{8}$$

$$\mathcal{W}_\phi=RW_\phi/K, \tag{9}$$

$$\mathcal{W}_\theta=RW_\theta/K, \tag{10}$$

$$\mathcal{F}=\frac{F}{K\pi l}, \tag{11}$$

where R and $l\gg R$ are the cylinder radius and length, respectively.

The corresponding volume free energy density is equal to

$$f_V=\frac{K}{2R^2}\left[\left(\frac{\partial\theta}{\partial\rho}\right)^2+\sin^2\theta\left(\frac{\partial\psi}{\partial\rho}\right)^2+\left(\frac{1}{\rho^2}+\mathcal{Q}'^2\right)\left(\frac{\partial\theta}{\partial\phi'}\right)^2+\left(\frac{1}{\rho^2}+\mathcal{Q}'^2\right)\sin^2\theta\left(\frac{\partial\psi}{\partial\phi'}\right)^2+\left(\frac{\sin 2\theta}{\rho}+2\mathcal{Q}'\sin^2\theta\sin\psi\right)\times\left(\frac{\partial\theta}{\partial\rho}\frac{\partial\psi}{\partial\phi'}-\frac{\partial\theta}{\partial\phi'}\frac{\partial\psi}{\partial\rho}\right)+\left(\frac{\sin 2\theta}{\rho}+2\mathcal{Q}\sin\psi\right)\frac{\partial\theta}{\partial\rho}+\mathcal{Q}\sin 2\theta\cos\psi\frac{\partial\psi}{\partial\rho}+\frac{2}{\rho}(\mathcal{Q}'\sin^2\theta-\mathcal{Q})\cos\psi\frac{\partial\theta}{\partial\phi'}+\left(\frac{2}{\rho^2}\sin^2\theta+\frac{\mathcal{Q}}{\rho}\sin 2\theta\sin\psi+2\mathcal{Q}\mathcal{Q}'\sin^2\theta\right)\frac{\partial\psi}{\partial\phi'}+\frac{\sin^2\theta}{\rho^2}+\frac{\mathcal{Q}}{\rho}\sin 2\theta\sin\psi+\mathcal{Q}^2\right], \tag{12}$$

and the surface free energy density is equal to

$$f_S=\frac{K}{2R}\left\{(\mathcal{W}_\phi\sin^2\psi+\mathcal{W}_\theta\cos^2\psi)\sin^2\theta-\mathcal{K}_{24}\left[\mathcal{Q}'\cos\psi\frac{\partial\theta}{\partial\phi'}+\left(\sin^2\theta-\frac{1}{2}\mathcal{Q}'\sin 2\theta\sin\psi\right)\frac{\partial\psi}{\partial\phi'}+\sin^2\theta\right]\right\}. \tag{13}$$

Minimization of the free energy with respect to variables θ and ψ yields a coupled system of a pair of partial differential equations:

$$\frac{\partial^2\theta}{\partial\rho^2}+\frac{1}{\rho}\frac{\partial\theta}{\partial\rho}+\left(\frac{1}{\rho^2}+\mathcal{Q}'^2\right)\frac{\partial^2\theta}{\partial\phi'^2}-\frac{1}{2}\left[\left(\frac{\partial\psi}{\partial\rho}\right)^2+\frac{1}{\rho^2}\left(1+\frac{\partial\psi}{\partial\phi'}\right)^2+\mathcal{Q}'^2\left(\frac{\partial\psi}{\partial\phi'}\right)^2+2\mathcal{Q}\mathcal{Q}'\frac{\partial\psi}{\partial\phi'}\right]\sin 2\theta+2\mathcal{Q}\left[\cos\psi\frac{\partial\psi}{\partial\rho}+\frac{\sin\psi}{\rho}\left(1+\frac{\partial\psi}{\partial\phi'}\right)\right]\sin^2\theta=0, \tag{14}$$

$$\frac{\partial^2\psi}{\partial\rho^2}+\left(\frac{1}{\rho}+2\cot\theta\frac{\partial\theta}{\partial\rho}\right)\frac{\partial\psi}{\partial\rho}+\left(\frac{1}{\rho^2}+\mathcal{Q}'^2\right)\frac{\partial^2\psi}{\partial\phi'^2}+2\left(\frac{1}{\rho^2}+\mathcal{Q}'^2\right)\cot\theta\frac{\partial\theta}{\partial\phi'}\frac{\partial\psi}{\partial\phi'}-2\mathcal{Q}\frac{\partial\theta}{\partial\rho}\cos\psi-\frac{2\mathcal{Q}}{\rho}\frac{\partial\theta}{\partial\phi'}\sin\psi+2\left(\frac{1}{\rho^2}+\mathcal{Q}\mathcal{Q}'\right)\cot\theta\frac{\partial\theta}{\partial\phi'}=0, \tag{15}$$

with the boundary conditions:

$$\left[\frac{\partial\theta}{\partial\rho}+(1-\mathcal{K}_{24})(\cot\theta+\mathcal{Q}'\sin\psi)\sin^2\theta\frac{\partial\psi}{\partial\phi'}+\frac{1}{2}(1-\mathcal{K}_{24}+\mathcal{W}_\phi\sin^2\psi+\mathcal{W}_\theta\cos^2\psi)\sin 2\theta+\mathcal{Q}\sin\psi\right]_{\rho=1}=0, \tag{16}$$

$$\left[\frac{\partial\psi}{\partial\rho}-(1-\mathcal{K}_{24})(\cot\theta+\mathcal{Q}'\sin\psi)\frac{\partial\theta}{\partial\phi'}+\frac{1}{2}(\mathcal{W}_\phi-\mathcal{W}_\theta)\sin 2\psi+\mathcal{Q}\cot\theta\cos\psi\right]_{\rho=1}=0. \tag{17}$$

Equations are solved numerically, and then the free energy is minimized with respect to the twist parameter $\mathcal{Q}'$.

In the case $\psi=-\phi'$, the AT model simplifies to the asymmetric conical director field with $\vec{n}=(\sin\theta\cos q'z,\sin\theta\sin q'z,\cos\theta)$ in Cartesian coordinates (see Ref. [8]). The difference between the two models is in the projection of the nematic director to the (x',y') plane which is aligned in the direction of x' axis in the AC structure and curved in the AT structure.

III. NUMERICAL SOLUTIONS

We focused our attention on the nematic director fields and corresponding free energies for different sets of material constants $\mathcal{K}_{24}$, $\mathcal{Q}$, $\mathcal{W}_\theta$, and $\mathcal{W}_\phi$. The influence of $\mathcal{K}_{24}$ and $\mathcal{Q}$ on the nematic structure is strong. $\mathcal{K}_{24}$ was varied from 0 to 2, while $\mathcal{Q}$ was varied from 0 to 30. We compared nematic director fields and free energies of AC and AT structures. In calculations of the stability regions of different structures, we also considered the free energies of RT and ERT structures. Finally we calculated and compared simulated polarization microscopy patterns of the structures.

A. Nematic director fields and free energies

First we calculated differences between natural chirality $\mathcal{Q}$ and actual chirality $\mathcal{Q}'$. The corresponding equilibrium free energies for AC and AT structure were evaluated for different sets of parameters. For both structures $\mathcal{Q}'$ is slightly smaller than $\mathcal{Q}$, but the difference between the chiralities and corresponding free energies is negligible except for low chiralities ($\mathcal{Q}<1$). Therefore, in further calculations we used the approximation $\mathcal{Q}'=\mathcal{Q}$ to reduce the computation time.

We limited our calculations of the axially twisted structures and the corresponding free energies to chiralities $\mathcal{Q}$ higher than 1 for two reasons. First, the nematic director tends to become highly aligned in the direction of the cylinder axis for lower chiralities. Equation (15) for the angle ψ is singular in the case of zero polar angle θ. This causes an ambiguity in the determination of the angle ψ at the points, where $\theta=0$, and also high numerical errors around such points. Therefore numerical solutions of the system of equations (14)–(17) are not reliable in the low chirality regime. Second, for low chirality, we expected the stability of a radially twisted structure with the nematic director: $\vec{n}=\cos\alpha(\rho)\vec{e}_z+\sin\alpha(\rho)\vec{e}_\phi$. Here α describes a twist of nematic director around the radial axis $\vec{e}_r$.

It should be noted that our form of the AT nematic director field described by Eq. (4) includes also the RT structure, if we set $\psi\equiv\pi/2$ and allow θ to depend only on ρ. In this case θ is equivalent to the twist angle α of the RT structure. We did not perform a complete calculation because of numerical problems mentioned above. Instead for low chiralities we took a simple RT structure (with the only parameter α depending on ρ) and obtained a discontionous transition to the AT structure with $\mathcal{Q}'=\mathcal{Q}$ at intermediate chiralities.

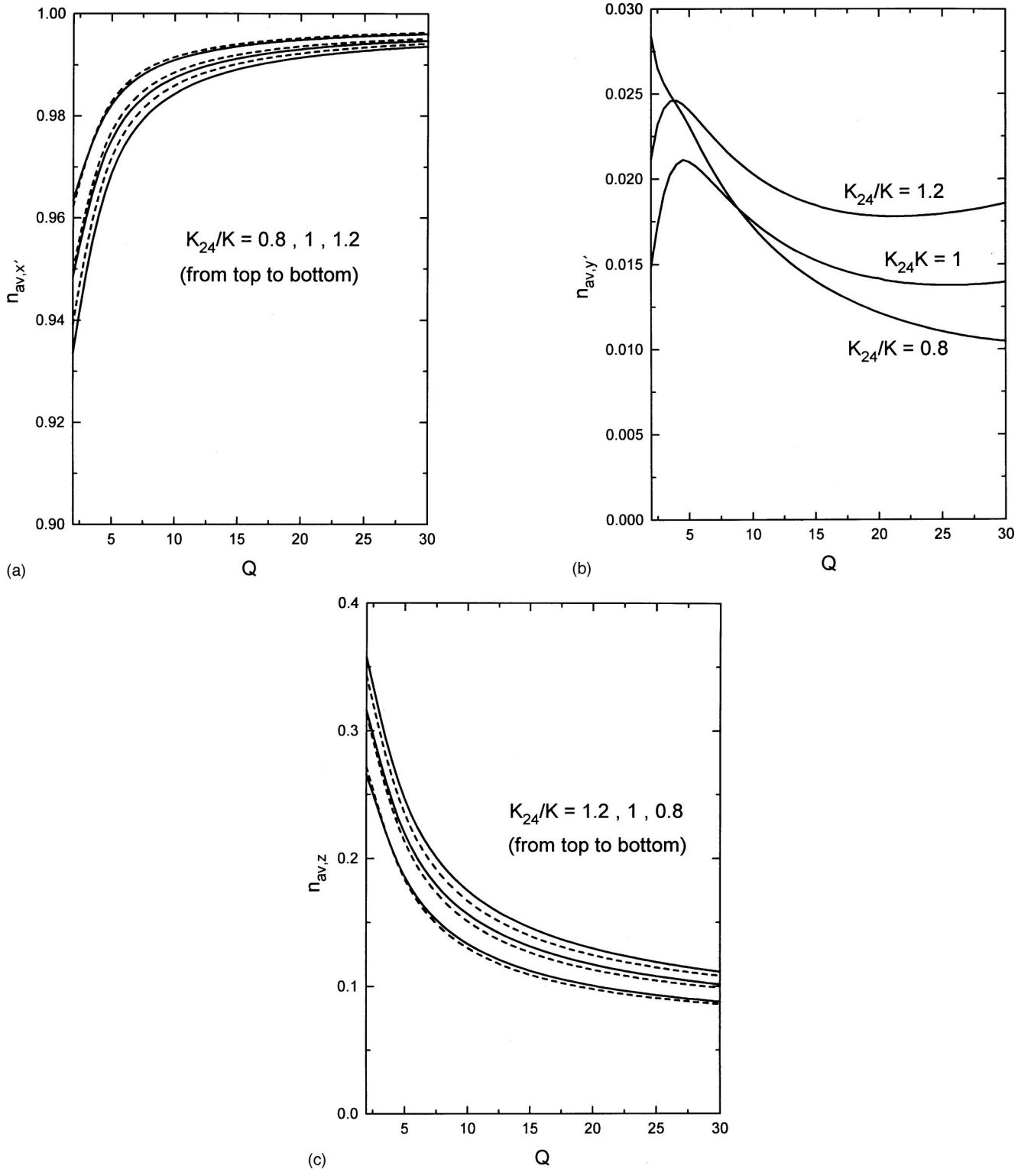

FIG. 2. Averaged nematic director components of AC (dashed lines) and AT (solid lines) structures. The components $n_{av,x'}$, $n_{av,y'}$, and $n_{av,z}$ are defined with respect to the rotating coordinate system (x',y',z). The material parameters are the following: $\mathcal{K}_{24}=0.8$, 1, or 1.2; $\mathcal{Q}=2-30$, $\mathcal{W}_\theta=1$; and $\mathcal{W}_\phi=0$. The nematic director component $n_{av,y'}$ for the AC structure is not shown because it is identically equal to zero.

AC and AT structures

We found that for higher chiralities $\mathcal{Q}>1$ the AC and AT structures are very similar. In both structures there is a rather small tilt of the nematic director out of (x',y') plane. It becomes significant only at a boundary layer. This has already been shown for the AC structure in Ref. [8]. Furthermore the projection of the nematic director to the (x',y') plane of the AT structure is nearly aligned, as in the case of AC structure. Both structures are thus similar to a simple

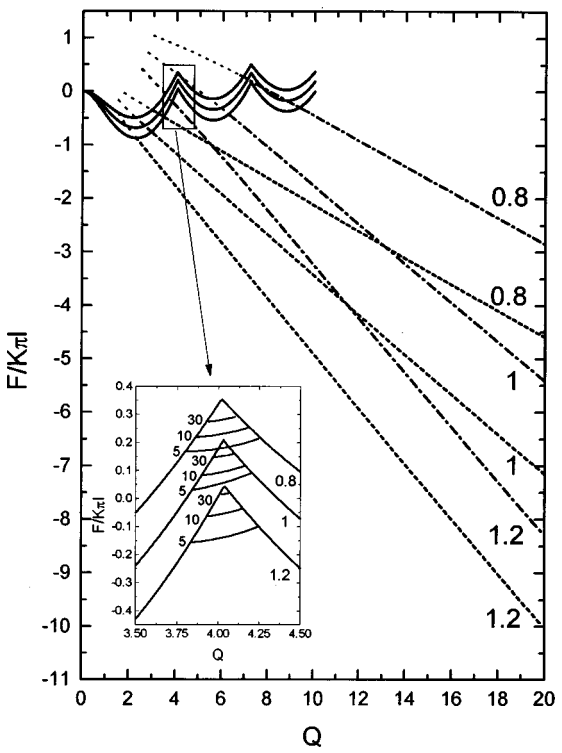

FIG. 3. Comparison of the chirality dependence of the RT and AT free energies. Numbers 0.8, 1, and 1.2 indicate $\mathcal{K}_{24}$ for AT lines. There are two lines for each $\mathcal{K}_{24}$, corresponding to two different values of polar anchoring strength: $\mathcal{W}_\theta=1$ for the lower (dashed) line, and $\mathcal{W}_\theta=5$ for the upper (dot-dashed) line. The AT lines are continued into dotted lines in the low chirality region, where the AT structure is unstable. $\mathcal{W}_\phi=0$ is zero. $\mathcal{K}_{24}$'s for the RT structure (solid lines), for curves from top to bottom, are 0.8, 1, and 1.2, while $\mathcal{W}_\theta$ does not influence the RT free energy. In the inset of the figure the free energies of RT and ERT around chirality $\mathcal{Q}=4$ are compared. The ERT structure depends, contrary to the RT structure, on anchoring strength; the cases with $\mathcal{W}_\theta=5$, 10, and 30 are shown.

planar helical structure, except in a boundary layer. In Fig. 2 the square roots of averaged squares of the three nematic director components for both structures are shown. We used the following symbols: $n_{\mathrm{av},i}=\sqrt{\langle n_i^2\rangle}$, where $\langle\cdots\rangle$ represents the average value of the quantity in brackets through the cylinder, and the subscript i stands for x', y' or z. We see that $n_{\mathrm{av},x'}$ has a value near 1 in both structures. In the helical structure, $n_{\mathrm{av},x'}$ is exactly 1. A small value of $n_{\mathrm{av},y'}$ in the AT structure means that it is similar to the AC structure, where $n_{\mathrm{av},y'}$ is identically equal to zero. The averaged director components are shown for chiralities between 2 and 30, for three different values of the saddle-splay elastic constant, and for the polar anchoring strength $\mathcal{W}_\theta=1$. The diagrams of averaged director components for higher anchoring strengths are similar to the ones in Fig. 2. In cases represented in Fig. 2 the azimuthal anchoring strength is taken to be zero. For nonzero $\mathcal{W}_\phi$ the difference between the two structures is even smaller. A small value of $n_{\mathrm{av},z}$ indicates a small average tilt of the nematic director out of the helical plane. The difference between the free energies of both structures is only a few percent. The free energies of the AT structure are shown in Fig. 3.

RT and ERT structures

The ERT structure was suggested in Refs. [1,6], on the basis of optical polarizing microscopy. Kitzerow *et al.* [6] called this structure the ''eccentric double twist structure.'' The structure is similar to an ordinary radially twisted structure. In the RT structure the nematic director on the cylinder z axis is parallel to the axis, and it twists around any radial axis on going away from the z axis. In the ERT structure the RT symmetry axis is deformed into a helix with radius r_h and pitch p_h winding around the z axis. At each point on the helix the nematic director is parallel to the z axis. We can consider the RT structure as a limiting case of the ERT structure with $r_h=0$. In Figs. 1(a) and 1(b) the nematic director fields of RT and ERT structures, with the helix radius equal to half the cylinder radius, are compared. The nematic director field of the RT structure is independent of the coordinate z, while for the ERT structure the whole helical planes twist around the z axis. In Ref. [6] the suggested model for the ERT structure (here written in our notation) was $\vec{n}=\cos\alpha(\rho')\vec{e}_z+\sin\alpha(\rho')\vec{e}_\phi$. It is of the same form as the director field for the RT structure, except that the reduced radius ρ' is now measured with respect to the new origin, which lies on the helix. In the simplest model the twist angle α is proportional to radius ρ'. However, this model does not fit boundary conditions well in the case of strong anchoring. Therefore, we slightly modified the model to decrease the surface anchoring energy: we added a quadratic term in ρ' to the function $\alpha(\rho')$, and further adapted the nematic director near the cylinder boundary to achieve a better fit with the preferred $(\vec{e}_\phi,\vec{e}_z)$ planar alignment. More details about the refinements of the model will be given elsewhere. We calculated the free energy of the ERT structure and compared it with the energies of RT and AT structures. Varying the saddle-splay elastic constant in the range $0.5<\mathcal{K}_{24}<1.5$, for intermediate values of $\mathcal{W}_\theta$ (roughly between 3 and 50) we found a stability region of the ERT structure for a chirality $\mathcal{Q}$ near 4. There the RT structure has a maximum (peak) of the free energy (Fig. 3). This prediction agrees with the experimental results of Kitzerow *et al.* [6] that the ERT structure is stable in the region where the helical pitch is of the order of the cylinder diameter. The transition from RT to ERT structure and back is discontinuous. For instance, in the case of $\mathcal{K}_{24}=1$, $\mathcal{W}_\theta=5$, and $\mathcal{Q}\approx4$, the radius of the helix r_h is about half the cylinder radius. With decreasing $\mathcal{W}_\theta$ the radius r_h increases, and, for instance, with $\mathcal{K}_{24}=1$, $\mathcal{Q}=4$, and $\mathcal{W}_\theta=\mathcal{W}_\phi=0$ one finds $r_h=0.95R$ and $p_h=8.6R$. In Fig. 3 it is seen that for small $\mathcal{W}_\theta$ (of the order of 1 or less) there is no ERT stability region, because the stability region of AT structures begins at a chirality less than 4. For $\mathcal{W}_\theta=5$ the AT stability region shifts toward higher chiralities, and so the ERT structures are stable for the values of chirality $\mathcal{Q}$ around 4. On the other hand, if anchoring is too strong ($\mathcal{W}_\theta>50$), the interval of chiralities around the energy peak of the RT structure, where the ERT structure becomes favorable, shrinks and disappears (inset of Fig. 3). There is a disagreement between our predictions and the experimental results in [6] for the optimal eccentric helix radius. Kitzerow *et al.* [6] reported that optical textures indicate that the helix radius is equal to the cylinder radius. Our calculations give about half as large a helix radius for anchoring strengths of order 5 and

higher. For very small anchoring strength ($\mathcal{W}_\theta \approx 0$) we also find $r_h \approx 1$, but the problem is that for this set of parameters the AT structures have lower free energy than the ERT structures.

B. Twist character of the structures

The twist character of chiral nematic structures can be quantitatively studied by using the twist pseudotensor introduced by Kilian and Sonnet [16]: $T_{ij} = \epsilon_{ikl} n_k n_{l,j}$. Here n_k are the components of the nematic director in the Cartesian coordinate system, and $n_{l,j}$ are their derivatives with respect to the coordinates. ϵ_{ikl} is the Levi-Civita antisymetric tensor of third rank. The convention of the summation over repeated indices is used.

The real nonzero eigenvalues of this tensor are the chiralities, and the corresponding eigenvectors give the directions of local twist axes. There can be zero, one, or two perpendicular local twist axes. For a single nondegenerate nonzero eigenvalue there is a twist of the nematic director around the single axis, as is the case for a simple chiral structure in unconfined chiral nematics. For a doubly degenerate eigenvalue we have a perfect double twist with eigenvectors forming a plane. In most cases we have two different eigenvalues (chiralities) with two perpendicular twist axes.

In RT structures the local twist axes are $\vec{e}_r$ and $\vec{e}_\phi$. On the cylinder axis the corresponding eigenvalues are equal (a perfect double twist). On approaching the cylinder boundary the twist around the $\vec{e}_r$ axis becomes more pronounced, indicating the transition from double- to single-twist character.

In ERT structures the two local twist axes also have components in the z-axis direction due to additional winding of the eccentric helix. Furthermore, points with a perfect double twist lie on the eccentric helix, but not on the cylinder axis.

In AC and AT structures we study twist character on the local y' axis, where the tilt of nematic director out of helical planes is the largest [Fig. 1(c)]. In both structures, at each point on the y' axis we have two twist axes: the z axis and the y' axis. The chirality around the z axis is nearly equal to the natural chirality. For a very high natural chirality $\mathcal{Q}$ the chirality around the y'-twist axis is negligible, except in a boundary layer. At points on the x' axis there is only a z-twist axis. Therefore, AC and AT structures are mainly single twisted.

C. Polarizing optical microscopy textures

Using calculated nematic director fields, we simulated polarizing optical microscope textures for radially twisted, eccentric radially twisted, and axially twisted structures. Optical microscopy is a useful tool for a study of director fields in cylinders with supramicrometer radii [1,17,18]. The textures were simulated with the aim to compare our results with experimental data. In Fig. 4, the textures are shown for the following parameters: $\mathcal{K}_{24}=1$, $\mathcal{W}_\theta=5$, $\mathcal{W}_\phi=0$, and $\mathcal{Q}=4$. The cylinder radius was taken to be 5 μm, while the incoming light wavelength was 435 nm, corresponding to the mercury light source. We took values of the ordinary and extraordinary refraction indexes for nematic liquid crystal $E7$: $n_o=1.544$ and $n_e=1.8208$ [17,18]. The direction of incident light is parallel to the y axis (perpendicular to the cylinder axis); therefore the textures are obtained in the xz plane. The incident light polarization is in the x direction, and the analyzer is set at an angle of 90° with respect to the incident polarization. The optical patterns of all three structures can be clearly distinguished from each other. In Fig. 5, a comparison of AT textures is shown for two different chiralities and two different polarizations. The textures are clearly distinguished from the simple helical structure textures (not shown in the figure, because there is no transmited light at all). The incident light polarization in Fig. 5 is in the x direction, and at an angle of 45° with respect to the x axis in the xz plane. In both cases, the analyzer is set at an angle of 90° with respect to the incident polarization. The material parameters are taken to be the same as in Fig. 4, except the chirality is now 5 and 10. The qualitative features of all AT textures are similar, except for smaller pitches in the z-axis direction in the case of higher chiralities. Other differences in patterns are too small to be noticed in Fig. 5.

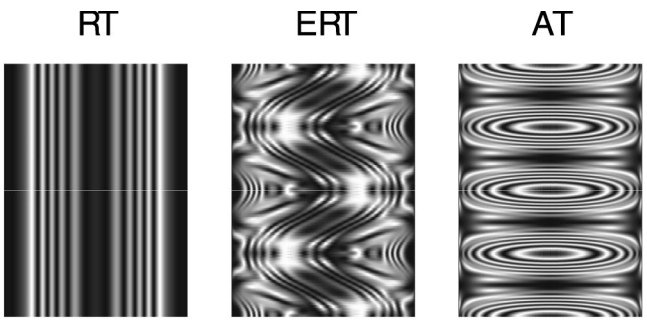

FIG. 4. Simulated optical polarizing microscope textures for RT, ERT, and AT structures. The material parameters are the following: $\mathcal{K}_{24}=1$, $\mathcal{W}_\theta=5$, $\mathcal{W}_\phi=0$, and $\mathcal{Q}=4$. The incident light polarization is parallel to the x axis.

IV. CONCLUSION

We studied axially twisted model structures of chiral nematic liquid crystals confined to cylindrical cavities with planar anchoring. The structure was shown to be similar to the previously studied asymetric conical structure. These two structures differ from a planar helical structure with a helical

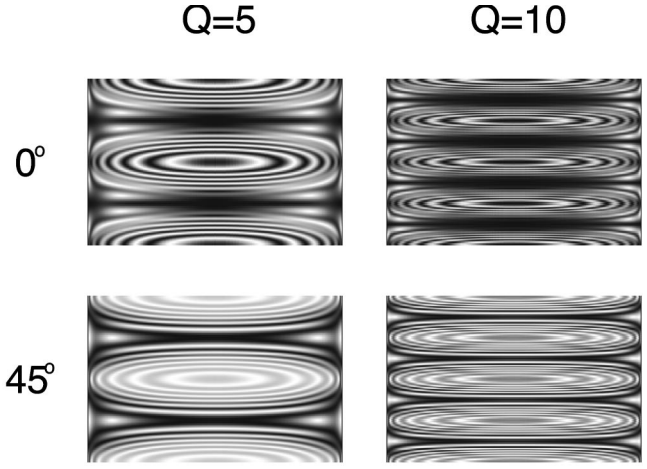

FIG. 5. Simulated optical polarizing microscope patterns for the AT structure for two different chiralities and two directions of the polarizer.

axis parallel to the cylinder axis in a tilt of the nematic director out of helical planes in a surface layer. Instead of taking the AT model, the structures can be described well enough by a single variable AC model, which allows simpler numerical calculations. The free energy of an AT structure is a few percent lower than the corresponding AC free energy. For low chiralities, the radially twisted structure is stable, except in the small interval of chiralities around the value $\mathcal{Q}=4$, where the eccentric radially twisted structure is stable for intermediate values of the polar anchoring strength. For high chiralities the axially twisted structure is stable. The K_{24} free energy term is deeply negative for high chiralities; therefore, the free energy of an AT structure is much lower than the free energy of a helical structure. This may significantly affect calculated stability phase diagrams of helical structures and blue phases [19], if helical structure is replaced by AT structure.

There remains a question of a possible stability of the ERT structure for higher anchoring strengths and for higher chiralities. A simple model of this structure does not allow its stability for very strong anchoring. A more advanced model which better optimizes bulk and surface free energies is needed to check this. Our simple ERT model has also revealed no existence of this structure for higher chiralities. The ERT structure might be expected to be stable at the chitalities $\mathcal{Q}\approx 7$, 10 etc., where the second, third, and higher energy maxima of the RT structure appear. However, the calculations so far show that AT structures have the lowest energies near higher RT energy peaks. There is a disagreement between our estimation of the radius of the helix of ERT structure and the results of Kitzerow *et al.* [6]. A possible explanation of the experiments of Kitzerow *et al*. would require a very weak anchoring at the cylinder surface and also a rather stable metastable ERT nematic structure, so that the stable reentrant AT structure would not develop with increasing chirality.

ACKNOWLEDGMENTS

This research was funded in part by the Ministry of Science and Technology of Slovenia under Project No. J1-0595-1554-98, and by the European Commission under Project No. INCO ERBCIPDCT940602.

[1] F. Lequex and M. Kleman, J. Phys. (Paris) **49**, 845 (1988).
[2] R. M. Hornreich and S. Strikman, Phys. Rev. A **41**, 1978 (1990).
[3] G. P. Crawford, D. W. Allender, and J. W. Doane, Phys. Rev. A **45**, 8693 (1992).
[4] R. J. Ondris-Crawford, G. P. Crawford, S. Žumer, and J. W. Doane, Phys. Rev. Lett. **70**, 194 (1993).
[5] H. Schmiedel, R. Stannarius, G. Feller, and Ch. Cramer, Liq. Cryst. **17**, 323 (1994).
[6] H. S. Kitzerow, B. Liu, F. Xu, and P. P. Crooker, Phys. Rev. E **54**, 568 (1996).
[7] R. J. Ondris-Crawford, M. Ambrožič, J. W. Doane, and S. Žumer, Phys. Rev. E **50**, 4773 (1994).
[8] M. Ambrožič and S. Zumer, Phys. Rev. E **54**, 5187 (1996).
[9] G. P. Crawford, L. M. Steele, R. J. Ondris-Crawford, G. S. Iannachione, C. J. Yeager, J. W. Doane, and D. Finotello, J. Chem. Phys. **96**, 7788 (1992).
[10] G. P. Crawford, D. K. Yang, S. Žumer, D. Finotello, and J. W. Doane, Phys. Rev. Lett. **66**, 723 (1991).
[11] M. Kleman, J. Phys. (France) Lett. **46**, L-723 (1985).
[12] J. D. Parsons and C. F. Hayes, Phys. Rev. A **9**, 2652 (1974).
[13] P. G. de Gennes and J. Prost, *The Physics of Liquid Crystals* (Clarendon, Oxford, 1993).
[14] F. C. Frank, Discuss. Faraday Soc. **25**, 19 (1985).
[15] B. Jerome, Rep. Prog. Phys. **54**, 391 (1991).
[16] A. Kilian and A. Sonet, Z. Naturforsch. Teil A **50**, 991 (1995).
[17] G. P. Crawford, J. A. Mitcheltree, E. P. Boyko, W. Fritz, S. Žumer, and J. W. Doane, Appl. Phys. Lett. **60**, 3226 (1992).
[18] R. D. Polak, G. P. Crawford, B. C. Kostival, J. W. Doane, and S. Žumer, Phys. Rev. E **49**, R978 (1994).
[19] S. Meiboom, J. P. Sethna, P. W. Anderson, and W. F. Brinkman, Phys. Rev. Lett. **46**, 1216 (1981).